

Transverse motions in sunspot super-penumbral fibrils

R. J. MORTON,¹ K. MOOROOGAN,¹ AND V. M. J. HENRIQUES^{2, 3, 4}

¹*Department of Mathematics, Physics and Electrical Engineering, Northumbria University, Newcastle Upon Tyne, NE1 8ST, UK*

²*Institute of Theoretical Astrophysics, University of Oslo, P.O. Box 1029 Blindern, N-0315 Oslo, Norway*

³*Rosseland Centre for Solar Physics, University of Oslo, P.O. Box 1029 Blindern, N-0315 Oslo, Norway*

⁴*Astrophysics Research Centre (ARC), School of Mathematics and Physics, Queen's University Belfast, BT7 1NN, Belfast, Northern Ireland, UK*

(Dated: Received /Accepted)

ABSTRACT

Sunspots have played a key role in aiding our understanding of magnetohydrodynamic (MHD) wave phenomenon in the Sun's atmosphere, and it is well known they demonstrate a number of wave phenomenon associated with slow MHD modes. Recent studies have shown that transverse wave modes are present throughout the majority of the chromosphere. Using high-resolution Ca II 8542 Å observations from the Swedish Solar Telescope, we provide the first demonstration that the chromospheric super-penumbral fibrils, which span out from the sunspot, also show ubiquitous transverse motions. We interpret these motions as transverse waves, in particular the MHD kink mode. We compile the statistical properties of over 2000 transverse motions to find distributions for periods and amplitudes, finding they are broadly consistent with previous observations of chromospheric transverse waves in quiet Sun fibrils. The very presence of the waves in super-penumbral fibrils raises important questions about how they are generated, and could have implications for our understanding of how MHD wave energy is transferred through the atmosphere of a sunspot.

Keywords: Sun: Chromosphere, waves, magnetohydrodynamics (MHD), Sun:oscillations

1. INTRODUCTION

It is well established that magnetohydrodynamic (MHD) waves are ubiquitous throughout the Sun's atmosphere, with evidence that they play key roles in energy transfer. A clear and beautiful example of their defining impact is found in the visual appearance and temporal evolution of the chromosphere, with slow MHD shocks driving chromospheric jets and mass loading events (De Pontieu *et al.* 2004). More recently, the identification of Alfvénic modes in the chromosphere and corona suggest these modes could supply a significant fraction of the required energy to explain the heating of the quiescent corona and acceleration of the solar wind (De Pontieu *et al.* 2007; Tomczyk *et al.* 2007; Jess *et al.* 2009; McIntosh *et al.* 2011; Morton *et al.* 2012a, 2015, 2019).

One of the outstanding questions around MHD wave propagation throughout the Sun’s atmosphere is, how are transverse wave modes excited? The fluctuations of velocity and magnetic field observed with both remote and in-situ sensing instruments suggest that Alfvénic waves exist over a wide range of time-scales. In the solar wind, Alfvénic fluctuations have time-scales on the order of at least a few hours (e.g., Goldstein *et al.* 1995). While in the solar chromosphere and corona, transverse wave modes with Alfvénic¹ characteristics (such as the long wavelength fast kink mode²) have, to date, only been identified unambiguously with much more modest time-scales ($\lesssim 2000$ s, e.g., Okamoto and De Pontieu 2011; Morton *et al.* 2012b; Weberg *et al.* 2020).

The current paradigm for the excitation of transverse waves largely focuses on the influence of the horizontal component of convection on photospheric magnetic fields. This mechanism for excitation is thought only to be relevant for wave excitation in small-scale magnetic elements, i.e., magnetic bright points, that exist with the internetwork and network, as well as plage. The convection generates transverse waves with time-scales on the order of 1 – 10 minutes, via the buffeting of the magnetic elements (Cranmer and van Ballegoijen 2005). This pathway for wave energy is a typical assumption for many wave-based numerical investigations that examine coronal heating or wind acceleration. However, there remain a number of issues associated with relying solely on transverse wave excitation at the photosphere, not least the large expected rate of reflection at the transition region due to steep gradients in the Alfvén speed (for a broader discussion see Cally 2017). Moreover, it is not evident how the near-surface convection leads to significant energy input at the larger time-scales found in the solar wind. Although, recently Cranmer (2018) discussed how magnetic reconnection could provide a contribution to wave generation in the corona from the evolution of the magnetic carpet.

An alternative suggestion that has been receiving increased attention focuses on the role of p -modes, which can inject additional energy into the corona through mode conversion. The theoretical description of this process implies that Alfvénic modes can be excited at the transition region (Cally 2011; Cally and Hansen 2011; Khomenko and Cally 2012; Cally 2017). There is also a clear power enhancement found at ~ 4 mHz in coronal Alfvénic velocity fluctuations (Morton *et al.* 2019) that could support the role of p -modes in exciting transverse waves. However, further investigation, both observationally and theoretically, is still required to demonstrate the efficacy of this energy pathway. For sunspots at least, this is potentially the only mechanism that could excite Alfvénic waves in the atmosphere that lies above.

Perhaps one of the best features on the Sun for studying MHD wave phenomenon are sunspots. Through observation and modelling, many aspects of MHD waves in inhomogeneous plasmas have been discovered and understood (e.g., Bogdan and Judge 2006; Jess *et al.* 2015, 2019). The source of MHD waves found in sunspots is largely considered to be from the internal p -modes, leaking out along the magnetic field. The p -modes are fast acoustic modes that convert to slow modes across the equipartition layer (where $c_s \approx v_A$). The slow modes observed in sunspots possess a clear signal of their origin, with a broad frequency distribution centred around a peak power of 3 mHz (e.g., Thomas *et al.* 1984). The sunspot’s strong magnetic fields provide a natural guide for slow magnetoacoustic modes. And their relatively simple structure makes it somewhat straightforward to undertake analysis of

¹ The phrase Alfvénic is used to refer to wave modes that have characteristics similar to the pure Alfvén mode. To quote Goossens *et al.* (2012), ‘[The kink waves are] to a high degree of accuracy incompressible waves with negligible pressure perturbations and with mainly horizontal motions. The main restoring force of kink waves in the magnetised flux tube is the magnetic tension force’. Hence, kink modes are Alfvénic in character.

² Goossens *et al.* (2012) demonstrate that total pressure perturbations for the kink mode are on the order of $(k_z R)^2$, where R is the flux tube radius and k_z the wavenumber.

observed fluctuations, reducing the complication of disentangling different waves modes (at least in the umbra).

The slow waves are observed to be channelled into the chromosphere and steepening as they propagate upwards (e.g., [Lites and Thomas 1985](#); [Brynildsen *et al.* 1999](#)), with the dominant frequency shifting to 5 mHz. Those waves propagating along the more vertical magnetic field in the sunspot umbra, with some wave-fronts steepening to shocks and producing umbral flashes in the chromospheric umbral atmosphere ([Roupe van der Voort *et al.* 2003](#); [Tian *et al.* 2014](#)). In the transition from umbra to penumbra, the dominant oscillatory pattern is the running penumbral waves ([Giovanelli 1972](#)), showing apparent propagation outward from the umbra. However, this apparent propagation is largely considered to be an illusion arising from upwardly propagating slow waves along inclined field lines ([Bogdan and Judge 2006](#); [Bloomfield *et al.* 2007](#)). The running penumbral waves show a frequency dependence with distance from the umbra, with the largest frequencies in the inner penumbra and decreasing outwards ([Briskin and Zirin 1997](#); [Kobanov and Makarchik 2004](#); [Jess *et al.* 2013](#)).

Both the shift in frequency of umbral oscillations and the change in dominant frequency of the running penumbral waves can be associated with the influence of gravitational stratification. The stratification of the atmosphere leads to the presence of an acoustic cut-off, which is modified by the plasma- β and the inclination of the magnetic field. The expression for the acoustic cut-off frequency, ν_c , in a high- β plasma is given by ([Bel and Leroy 1977](#)):

$$\nu_c = \frac{\gamma g \cos \theta_B}{4\pi c_s}, \quad (1)$$

where γ is the ratio of specific heats, g is the gravitational constant, and c_s is the sound speed. Hence, as the sunspot magnetic field becomes more inclined in the penumbra, this reduces the effective stratification and hence lowers the cut-off frequency. Therefore lower frequency waves are able to propagate into the chromosphere further from the umbra.

Slow magnetoacoustic modes are not the only MHD mode expected to be present in the sunspot atmosphere. The inclination of the field enables the conversion of the fast acoustic modes to fast magnetoacoustic modes at the equipartition layer, with the amount of conversion dependent upon inclination and attack angle of the waves (e.g., [Schunker and Cally 2006](#)). The presence of fast wave modes is now a well established feature of numerical simulations of sunspots (e.g., [Khomenko and Collados 2006](#)), but their presence has so far been inconspicuous in observations. To date, the only signature of their existence has been inferred from an enhancement of high-frequency (5.5-7.5 mHz) wave power surrounding active regions ([Brown *et al.* 1992](#)), which has been explained in terms of fast mode refraction due to the increase in Alfvén speed in the sunspot atmosphere ([Khomenko and Collados 2009](#)). Moreover, the production of fast modes at the equipartition layer is a key step in the generation of Alfvénic modes at the transition region.

It is hopefully apparent that identifying fast modes in the sunspot atmosphere will be a key step in confirming or challenging the current paradigm around wave energy transfer through p -modes. Such results would enable further studies of the typical properties of the fast modes, permitting an assessment of whether existing intuition about mode conversion within a sunspot is correct. While the fast mode has been difficult to detect through analysis of intensity variations and Doppler velocities, an examination of the fine-scale structure of the sunspots chromosphere, i.e., super-penumbral fibrils,

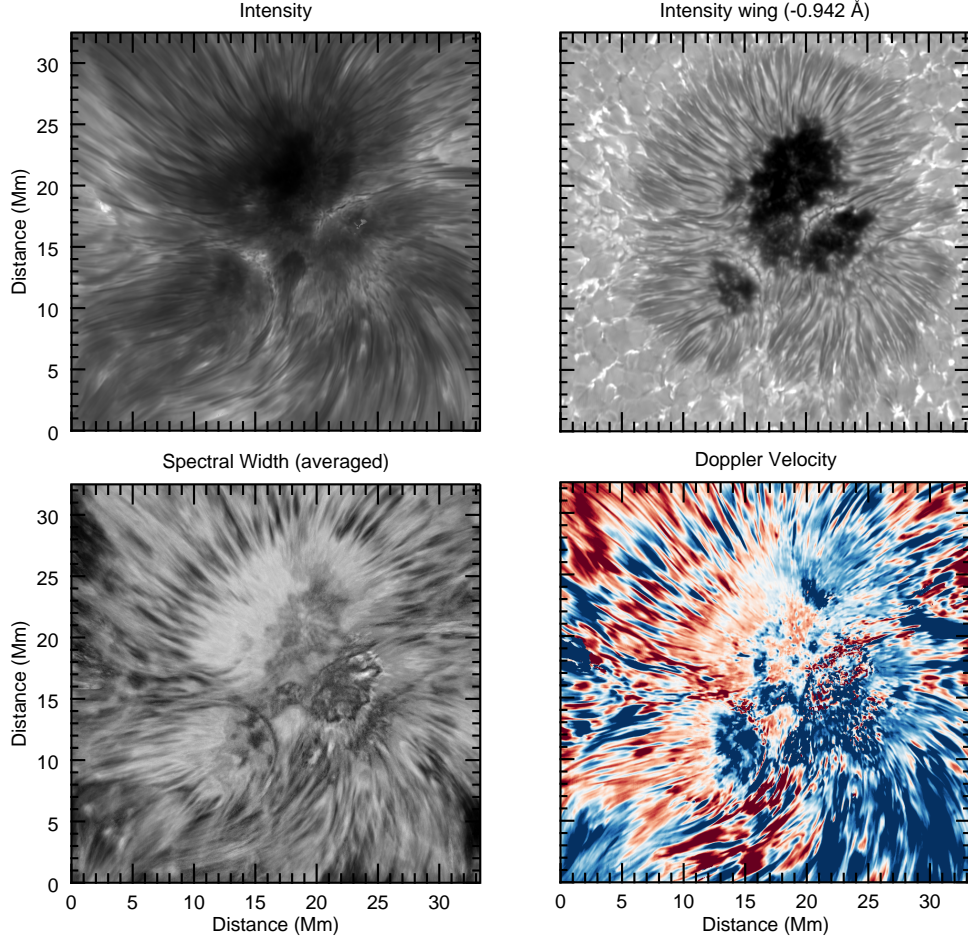


Figure 1. The sunspot as observed in Ca II 8542 Å. The upper left image shows the chromospheric emission at the nominal line centre wavelength. Super-penumbral fibrils are seen to extend near-radially from the chromospheric umbra in the upper half, while those in the lower half are more curvilinear. The upper right-hand image shows the photospheric section of the sunspot as observed in the wings of the Ca II line (-0.942 Å). The lower two panels show the temporally averaged line width (left) and Doppler velocity (right) data products. The width and Doppler components of the fibrils can be seen in both data product images.

may be able to provide some direct evidence for their existence. Here, we demonstrate that super-penumbral fibrils display ubiquitous transverse motions, which we interpret as the MHD kink mode. The observed motions are localised to individual fibrils, rather than being a global motion of the sunspot itself. The presence of kink modes in a structured sunspot atmosphere would provide support for current picture of energy transfer through the mode-conversion of p -modes.

2. OBSERVATIONS AND DATA REDUCTION

The observation presented here are focused on an active region sunspot close to disk centre $N 9.25, W 4.50$ (Figure 1), taken by the Swedish Solar Telescope (Scharmer *et al.* 2003, SST -) using the CRisp Imaging SpectroPolarimeter (CRISP - Scharmer 2006; Scharmer *et al.* 2008) on 28 July 2014 between 10:43 and 11:24 UT. The data set is a full Stokes polarimetric scan of the Calcium II 8542 Å infrared triplet line at fifteen wavelength positions in the range $\pm(0.942, 0.580, 0.398,$

0.290, 0.217, 0.145, 0.073, 0) Å from line centre. Further technical details with regards to acquisition and processing can be found in [Henriques *et al.* \(2017\)](#).

The data has the a spatial sampling on the order of $\sim 0''.059$ per pixel (spatial resolution $0''.21$). The data were processed with an early version of the CRISPRED pipeline ([de la Cruz Rodríguez *et al.* 2015](#)), centred around multi-object multi-frame blind deconvolution (MOMFBD [van Noort *et al.* 2005](#)) using an extended scheme as in [Henriques \(2012\)](#). The data was then de-rotated, aligned, and de-stretched ([Shine *et al.* 1994](#)).

Here we concentrate on the Stokes I component of the data, and use it to estimate the line profile minimum (LPM) intensity³, Doppler shift and width of the Ca II line (Figure 1). Due to the steep wings of the Ca II line profile, a Voigt profile is used to model the spectral profile for each pixel and all time-frames. The Voigt profile has the form,

$$V(\lambda : \sigma, \gamma) = \int_{-\infty}^{\infty} G(\lambda, \sigma) L(\lambda' - \lambda, \gamma_L) d\lambda,$$

where $G(\lambda, \sigma)$ is a Gaussian profile, $L(\lambda' - \lambda, \gamma_L)$ is a Lorentzian and λ' is the displacement from line centre. As it can be seen the Voigt profile is a convolution of Gaussian and Lorentzian profiles, taking into account both thermal and collisional broadening mechanisms respectively. These manifest in the parameters, γ_L and σ , that refer to the collisional and Doppler broadening mechanisms respectively. Both of these parameters contribute to the width of the line. The Voigt profile is fit to each Stokes I profile using least-squares minimisation (`mpfit`; - [Markwardt 2009](#)). After fitting the Voigt profile, we use the σ parameter as a proxy for exploring thermal variability, whilst ignoring the collision contributions. There were two missing time-steps in the Stokes I data and there also was a small variation in cadence. For each derived data product, the data sequence is homogenised to a cadence of 30 s and missing time-steps filled using spline interpolation for a total of 81 frames.

3. COMPRESSIVE WAVES

As discussed in the introduction, sunspots are well known to host a variety of wave phenomenon, which are often related to the slow magnetoacoustic wave modes and thought to be due to the leakage of the internal acoustic modes into the atmosphere. This sunspot is no different. While not our main focus, we give a brief overview of the compressive wave phenomenon that is visible in the data. Furthermore, we exploit their presence to undertake some basic magneto-seismology that aids our later discussion.

3.1. *Observational signatures*

Figure 2 captures the key features on the compressive phenomenon within the umbra and penumbra. In the chromospheric umbra we see clear evidence for the upward propagating slow waves, which are marked most strikingly by the periodic red and blue shifts with periods of 6-7 mHz (determined from Fourier analysis of the time-series). There is a large-scale bowl-shaped pattern for each wave front in both intensity and Doppler shift (Figure 2). The slow waves first appear close to the sunspot centre and show an apparent outward propagation into the penumbral regions. The ‘sides’ of the bowl represent the innermost component of the running penumbral waves. As already discussed,

³ The line profile minimum images enable us to disambiguate the velocity effects that are introduced by using the intensity recorded at a single wavelength position in the line scan, e.g., nominal line core.

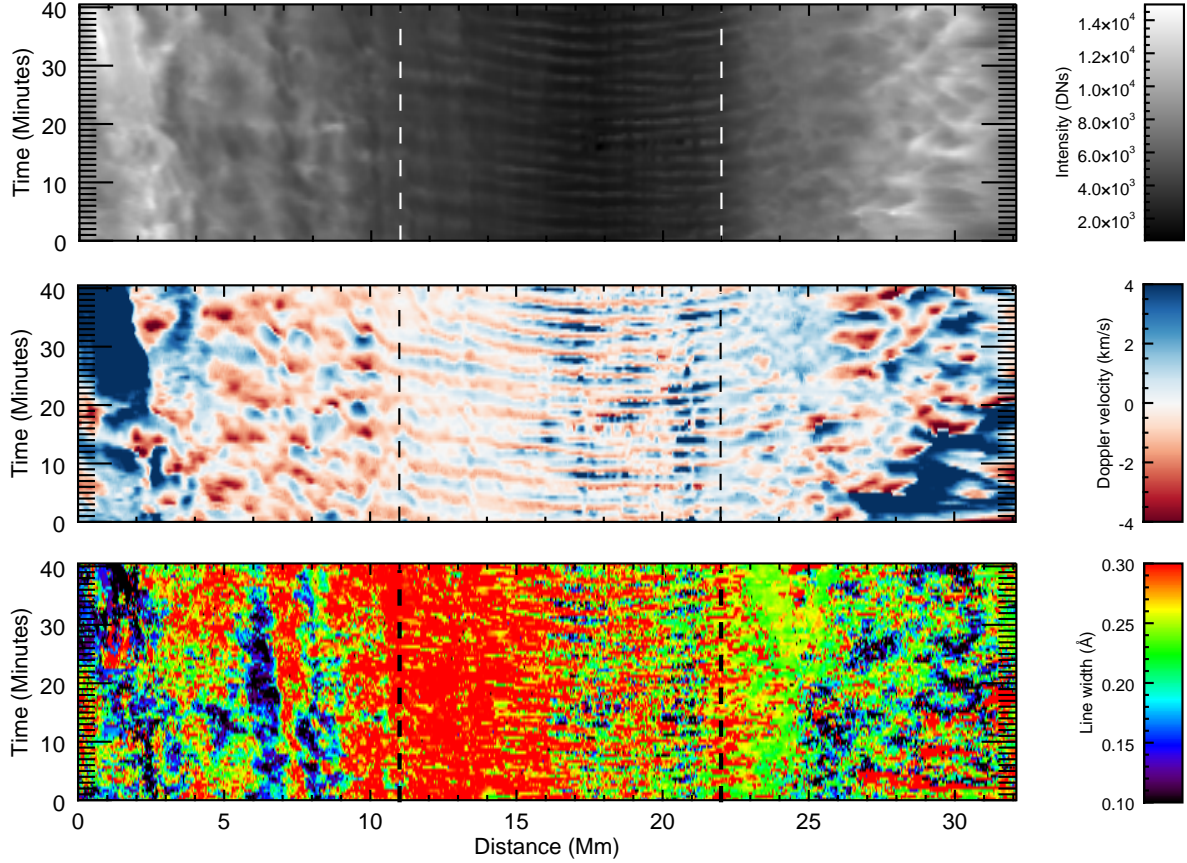


Figure 2. Co-spatial time-distance diagrams that reveal the presence of slow magnetoacoustic oscillations. The figure displays trans-sunspot time-distance diagrams of the LPM intensity, Doppler velocity and Doppler line width (from top to bottom respectively). The slow modes can most clearly be identified by the alternating ridged pattern most evident near and through the umbra (area between vertical dotted lines).

this apparent propagation is considered to be an illusion arising from upwardly propagating slow waves along inclined field lines (Bogdan and Judge 2006; Bloomfield *et al.* 2007). The near-vertically propagating waves reaching the region of the atmosphere that contributes to Ca II line formation first, followed by waves propagating along the inclined fields.

In addition to the spot-wide intensity and velocity fluctuations, there is also visible signatures of the umbral flash phenomenon, marked by saturated blue shifts to the right-hand side of the umbra. We also see that the shocks broaden the Calcium line profile. Due to the mass of the calcium atom, the line is sensitive to non-thermal broadening (Cauzzi *et al.* 2009), hence the observed broadening could either be a signature of plasma heating or turbulence generated by the shocks.

3.2. Slow wave magneto-seismology

In advance of our discussion, we would like to obtain an impression for the inclination of the magnetic fields around the sunspot. If we take forward the assumption that the running penumbral waves are upwardly propagating slow waves along inclined field lines, Bogdan and Judge (2006) suggested that one can use the frequency values of the slow waves with the largest power, ν_{max} , to map the inclination of the magnetic field (see Löhner-Böttcher 2016, for a full discussion and an implementation of this method).

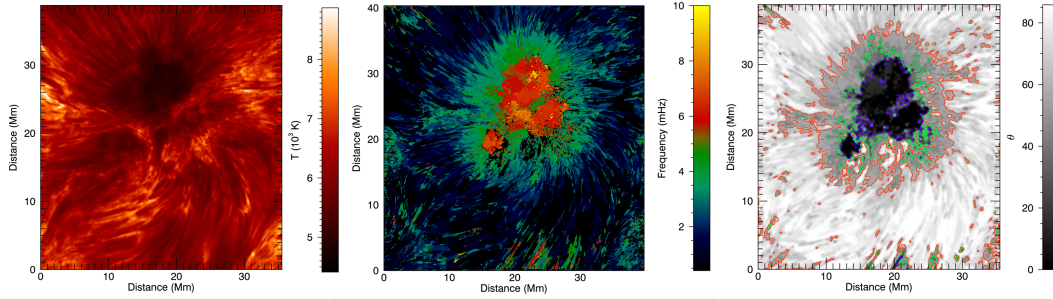


Figure 3. Estimating magnetic field inclination in the sunspot. The left panel is the estimated temperature of the chromosphere. The middle panel shows the frequency values with the largest power in each pixel for the Doppler velocity time-series. The right-hand panel displays the estimated inclination angle of the magnetic field with respect to the vertical. The overplotted contours mark inclinations of 20° (blue), 40° (green) and 60° (red). Note that the inclination map has been averaged with $0''.7$ box-car filter to aid visualisation.

The inclination of the magnetic field, θ_B is given by

$$\theta_B = \cos^{-1} \left(\frac{4\pi\nu_c}{g} \sqrt{\frac{RT}{\gamma\bar{\mu}}} \right) \quad (2)$$

where R is the molar gas constant, $\bar{\mu}$ mean molar mass (which we take as 1.26 for a weakly ionized solar plasma), T is the plasma temperature. The key to using Equation (2) is finding a relationship between ν_c and ν_{max} . [Löhner-Böttcher \(2016\)](#) used an empirical relationship, $\nu_{max} \approx C_{emp}\nu_c$, where $C_{emp} = 1.25$ was suggested by [Bogdan and Judge \(2006\)](#). However, this relationship is based upon the maximum frequencies found at the umbral centre in the observations used by [Bogdan and Judge \(2006\)](#), with the assumption that $\nu_c = 5.2$ mHz and maximum frequencies are between 6-7 mHz. There will be some need to alter C_{emp} based upon the observed values of maximum frequency found in each spot, otherwise the above formula does not perform well. The inversion relationship, ignoring the standard constants, comes down to

$$\cos \theta_B \propto \frac{\nu_{max}\sqrt{T}}{C_{emp}}, \quad (3)$$

and it is clear that an issue which can arise is relatively large values of ν_{max} lead to the RHS being larger than 1. The frequency values for which this occurs will also be influenced by the estimated temperature too. This means that a modification of C_{emp} is required to get the best results for the inversion. Here we find that $C_{emp} = 1.35$ gives reasonable results for this sunspot, although, umbral pixels with the largest ν_{max} (> 7 mHz) still cause issues and inversion angles are set to 0 degrees. We discuss what we believe to be the reason for this in the following paragraph.

Applying Fourier analysis on a pixel-by-pixel basis across the FOV, maps are produced that show the frequency value at which the power of the oscillations is found to be largest (Figure 3). This is performed on both intensity and velocity data, however, it is found that the intensity power maps are dominated by the lowest frequencies outside of the umbra - potentially due to long-term variations

in the sunspot atmosphere. Hence, unlike Löhner-Böttcher (2016), we use the maximum frequencies from the Doppler velocity data (Figure 3 middle panel). In the umbral sections, higher-frequency magnetoacoustic power can be seen to be dominant, with most of the umbra having periodicities of 6 – 7 mHz. As expected, the frequency of maximum power decreases in the transition from umbra into penumbra. Away from the sunspot, low-frequency power dominates, which is probably due to long-term evolution of the plasma velocity. As mentioned above, a few umbral regions show the largest power is at frequencies greater than 7 mHz. Inspection of the data suggests that the largest ν_{max} values come from locations where the Doppler velocity time-series has strong discontinuities, which could cause enhanced high-frequency power in a discrete Fourier transform. It would appear that these sharp changes in velocity are artefacts arising from the model fitting of the line profile. Given we are primarily interested in finding the inclination of the super-penumbral fibrils rather than the inclination across the spot, the pixels with affected Doppler time-series are not an issue. Needless to say, the interpretation of the results from these regions should be undertaken with caution.

3.3. Temperature estimates

Temperature maps were produced using semi-empirical modelling with the Non-LTE Inversion COde using the Lorien Engine (NICOLE; Socas-Navarro *et al.* 2015). Due to the large FOV and limited computing resources, only one inversion cycle was run. Per parameter, the following equidistant node scheme was used: Temperature - 8, LOS Velocity - 3, Microturbulence - 1, Magnetic field (each Cartesian component) - 1. The starting model was the “FAL-C” model (Fontenla *et al.* 1993) and the reference for line-core wavelength calibration was a patch of quiet Sun. The latter choice differs by only 120 m s^{-1} from selecting a time average over the umbra for these observations (Henriques *et al.* 2020). NICOLE was run without modifications and the following key settings were selected: three rays for the non-LTE computation cycle with LTE starting populations (a compromise between speed and accuracy), cubic DELO-Bezier solver for the radiative transfer equation (de la Cruz Rodríguez and Piskunov 2013), and isotopes for the Ca atom model included as in Leenaarts *et al.* (2014). The inverted temperatures were averaged around the formation height of the Ca II 8542 Å line core. For the penumbra, at a μ of 0.745, this height is around $\log \tau_{500} = -5.5$ (Bose *et al.* 2019). Given the higher μ in this work we followed a simple average at $\log \tau_{500} = -5 \pm 1$. Very little noise is present in the temperature maps which is due to very few pixels showing strong local divergence of solutions (i.e. the “inversion noise” is low).

Figure 3 displays the estimated temperature (left panel) and LOS inclination estimated using Eq. 2 (right panel). As can be seen in the LOS inclination map, the umbral field is near vertical and the angle to the vertical increases from the umbra to super-penumbra. The super-penumbral fibrils have inclinations around 40-70°.

4. TRANSVERSE MOTIONS

Spanning out near-radially from the umbra are the chromospheric super-penumbral fibrils. Previous studies of the fibrils enables us to state some of their basic properties. Through spectro-polarimetric observations of Ca II 8542 Å, Asensio Ramos *et al.* (2017) demonstrated the dark fibrils in sunspot penumbra largely align with the magnetic field orientation. This is also supported by alignment between the thermal and magnetic structure inferred from He 10830 Å observations of super-penumbral fibrils (Schad *et al.* 2013). Moreover, Schad *et al.* (2015) suggest that the lateral structure of the

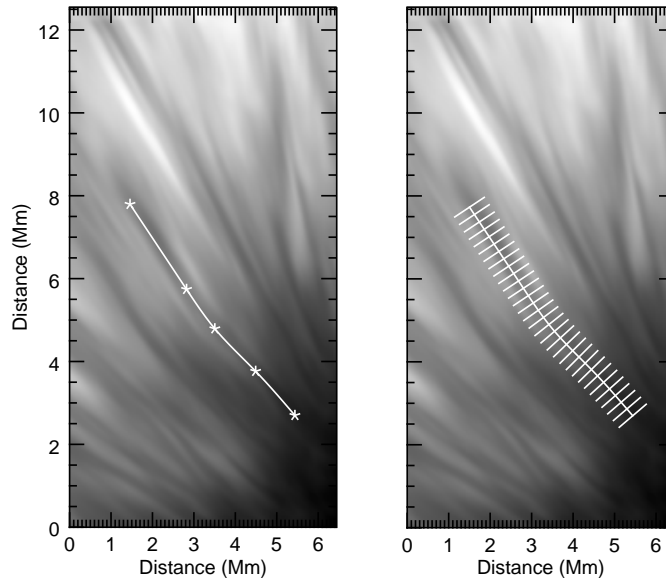


Figure 4. An isolated set of fibrils in the Ca II sunspot super-penumbra. The left panel of the figure shows the manually selected guide points (white stars) and the resulting outline of the fibril’s central axis is over-plotted. In the right panel, the cross-cuts normal to the guide-line is shown along the fibril structure. For clarity a small number of guide points and a large separation distance is chosen.

magnetic field throughout the penumbral chromosphere is relatively homogeneous, implying that the observed inhomogeneities are due to density or temperature. The reduced intensity of the fibrils suggest that the plasma has greater opacity at 8542 Å (and in other chromospheric lines) than the surrounding plasma, suggesting it is denser than the ambient plasma. Moreover, as was demonstrated with the slow mode magneto-seismology, the magnetic field aligned with the observed fibrils was found to be inclined from the vertical. The implication of this is that the fibrils are field-aligned density enhancements, providing wave-guides that can define MHD wave propagation.

Due to high spatial resolution of this data set (and high signal-to-noise), we are able to follow the motions of these fibrils and find evidence of quasi-periodic transverse motions.

4.1. *Individual fibrils*

First, we focus on a few examples to demonstrate the features of the transverse motion. The examples are selected because the fibril is visible for a significant portion of the data set.

In order to follow the propagation of the transverse motion, we trace out what we believe to be the magnetic axis. The time-average of the LPM images are used (averaged over 2400 s) to determine the average location of the fibrils and a curvilinear path is defined that follows the central axis. Figure 4 demonstrates an example of a cubic spline fitted to the longitudinal axis of the fibril. Cross-cuts normal to this curve are then taken, shown by the white lines in the right hand panel.

The cross-cuts are used to generate time-distance diagrams from the full LPM image time-series. Figure 5 displays time-distance diagrams generated from cross-cuts taken across three separate fibrils located around the sunspot. Each one is seen to support transverse motions ⁴ (right panel), high-

⁴ We note that manifestations of the slow magnetoacoustic waves can be seen as intensity ridges (lower right panel Figure 5). Features like this are most evident in time-distance plots that originate closer to the umbra.

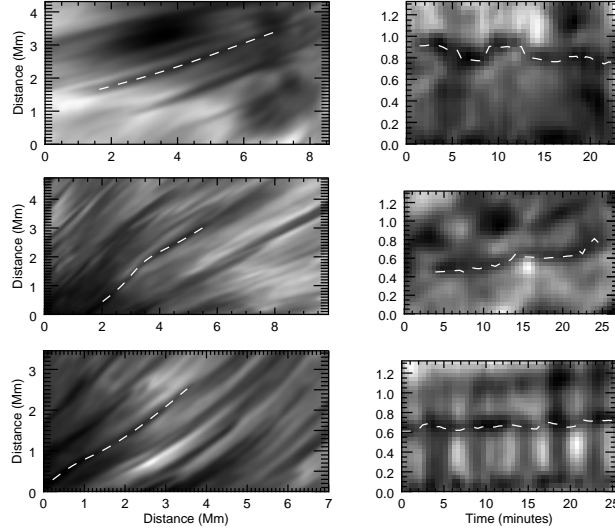


Figure 5. Examples of a fibril showing transverse motions. The left-hand panel displays the fibril and the trace of its axis. The right hand panel is a time-distance diagrams from a perpendicular cross cut, with the dashed line indicating the central location of the fibril axis over time.

lighted by the white curve that shows the central location of the fibril’s axis. The location of the centre of the fibril axis is found by a fitting a Gaussian function to the intensity values of the fibril’s cross-sectional profile in each time frame (see e.g., Morton 2014; Morton *et al.* 2014; Mooroogen *et al.* 2017). The uncertainties on the intensity values are used in the fitting process and estimated following the method described in Mooroogen *et al.* (2017).

The fibrils are observed to undergo a transverse displacement, with the displacements showing coherent motion along the length of the fibril, i.e., the longitudinal axis moving nearly in unison. In Figure 6 we show a series of displacement time-series for one fibril, each taken from locations along a fibril’s longitudinal axis. As is seen in Figure 5 and Figure 6, the displacements of the fibril are typically relatively small, on the order of ~ 100 km; which is similar to the scale of kink waves seen in chromospheric fibrils in other regions of the Sun’s atmosphere (Morton *et al.* 2014; Jess *et al.* 2015; Jafarzadeh *et al.* 2017). The fibril is seen to support a number of short wave packets that lead to near-sinusoidal transverse motion⁵. The evolution of the wave packets can be seen to be relatively rapid, increasing or decreasing in amplitude over short distances. This behaviour has been seen previously in quiet Sun (Kuridze *et al.* 2013) and plage (Jafarzadeh *et al.* 2017) observations of chromospheric transverse motions. Given this, we interpret the motions observed here as signatures of transverse waves, namely the MHD kink mode.

Following the method described in Mooroogen *et al.* (2017), we estimate propagation speeds for the transverse motions supported by ten individual fibrils. Interestingly, much like the internetwork fibrils examined in Mooroogen *et al.* (2017), the propagation speeds appear to be invariant over the fibrils’ length. Figure 7 displays a histogram of the measured propagation speeds and they are summarised in Table 1. The propagation speeds are less than that found in the quiet Sun and internetwork fibrils (Pietarila *et al.* 2011; Morton *et al.* 2012b; Kuridze *et al.* 2013; Mooroogen

⁵ By near-sinusoidal we mean that the fibril is seen to sway back and forth, with a displacement time-series that could be predominantly described by a sinusoidal function. Although, typically there is some deviation from a pure sinusoid.

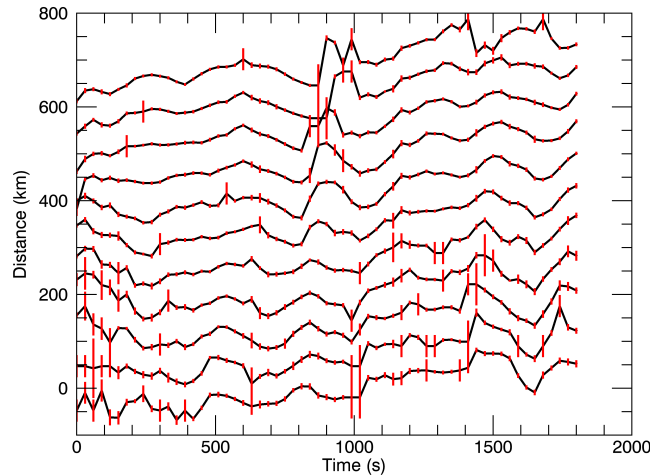


Figure 6. Displacement time-series from along a single fibril shown in Figure 4. Black curves relate to the measured central location of the fibril cross-section, while the red vertical lines show the 1 sigma uncertainties on each measurement. Each series is measured at 150 km intervals along the longitudinal axis of the fibril. The series are off-set by an arbitrary amount for visualisation

et al. 2017), although they are similar to those found in Ca II H slender fibrils (SUNRISE - Jafarzadeh *et al.* 2017; Gafeira *et al.* 2017). The expected sound speed in the sunspot chromosphere is $\sim 6 - 10 \text{ km s}^{-1}$ (estimated from the temperature inversions), and all measured values are larger than this. In principle, the larger magnetic field strengths in active regions ($\sim 300 - 400 \text{ G}$ - Asensio Ramos *et al.* 2017) should lead to larger Alfvén speeds than we observe. Given the inclination of the field lines, we are likely underestimating the length of the fibrils due to projection effects leading to smaller values of propagation speeds. Although, considering the map of inclination angles obtained for the sunspot (Figure 3), the length is likely underestimated by around 15-50 % (inclination of $40-70^\circ$ to the vertical) - leading to a comparable increase in propagation speeds.

With the cadence of this data set at 30 s, the temporal resolution is really at the upper limit to provide a detailed analysis of the transverse motions. In general, it is not possible with this data set to find many examples where the propagation of the transverse motions along the fibrils can be measured with certainty. Under the assumption of wave motion, e.g., the kink mode, the displacements would propagate at typical Alfvén speeds of $\sim 100\text{'s km s}^{-1}$. Moving at such speeds would lead to small lags between neighbouring cross-cuts that would be difficult to find, at least with the current methodology. Moreover, examining movies of the data reveal that the fibrils can disappear and reappear (this behaviour is also visible in the time-distance diagrams), much like the internetwork fibrils in Moorooogen *et al.* (2017) but on longer time periods⁶. Hence this places further limits on following wave motions. This restriction is not limited to measuring propagation; for example, the dominant periods from measurements of transverse waves in other fibrils are around 100-150 s (Morton *et al.* 2014) corresponding to $\sim 3-5$ time-frames here.

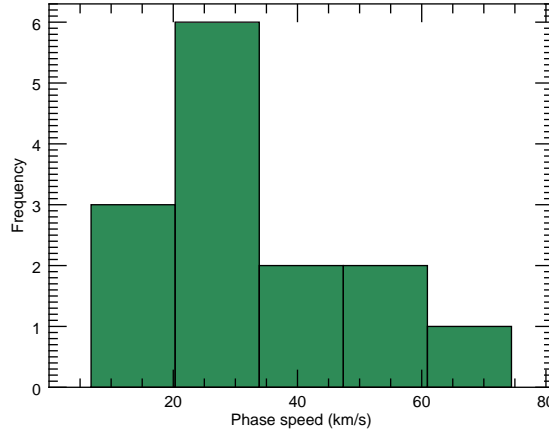
⁶ We do not examine the reasons behind the fibril visibility, but suggest it could be the result of mass-loading events leading to variability in the fibril density (Chae *et al.* 2014, 2015; Leenaarts *et al.* 2015), and hence opacity in Ca II.

Table 1. Super-penumbral fibril transverse wave properties

| | Mean | Median | Mode | σ^\dagger | n^* |
|--------------------|------|--------|------|------------------|-------|
| Displacement (km) | 74 | 62 | 46 | 47 | 2306 |
| Period (s) | 754 | 570 | 330 | 529 | 2306 |
| Velocity (km/s) | 0.76 | 0.66 | 0.34 | 0.47 | 2306 |
| Prop. speed (km/s) | 25 | 21 | - | 0.74 | 10 |

† Standard deviation

* number of measurements

**Figure 7.** Distribution of phase speeds. Histogram showing the distribution of phase speeds of the ten isolated super-penumbral fibrils.

The transverse motions are not limited to the ten features studied in this section; they are found to be ubiquitous through the super-penmbtral fibrils. In order to provide a broader picture of the transverse motion in the super-penumbra, we will utilise an automated method to undertake further measurements ([Weberg *et al.* 2018](#)).

4.2. General properties

To reveal how wide-spread these motions are, we define arcs that are at a fixed distance from the sunspot umbral bary-centre. These arcs sample the fibrils located in upper half of the sunspot, where the fibrils are largely aligned radially. Hence, the tangents to the arc are largely perpendicular to the fibrils' longitudinal axis. The arcs do not cover the lower half of the spot as fibrils are more curved and not always radially orientated. To remove large-scale spatial variations of intensity and improve visibility of the fibrils, we implement two-dimensional square box-car filter of side-length $0''.9$ in order to unsharp mask the data. Figure 8 shows an example of the time-distance diagrams obtained from critically sampling the data along the arcs. By zooming in on the figure it can be seen that most of the dark super-penumbral fibrils are subject to some transverse motion, with some showing clear near-sinusoidal displacements.

To measure the typical properties of the kink waves, we use the NUWT code. We provide here a cursory summary of the methodology but refer readers to [Weberg *et al.* \(2018\)](#) for a detailed

discussion. In each time-distance diagram, the fibril centers are located. A sub-pixel estimate of the location is obtained by approximating the cross-sectional structure as a Gaussian and finding the best model parameters via weighted non-linear least squares. Uncertainties on intensity values were calculated via the methodology discussed in [Moeroogen *et al.* \(2017\)](#). By following each fibril in time, a displacement time-series can be constructed. Each of these time-series is then subject to a Fourier decomposition, and the amplitude and period of the dominant Fourier mode is obtained. A lower limit is placed on the length of time-series in order to keep noisy time-series to a minimum; the shortest time-series here are of length 10 samples.

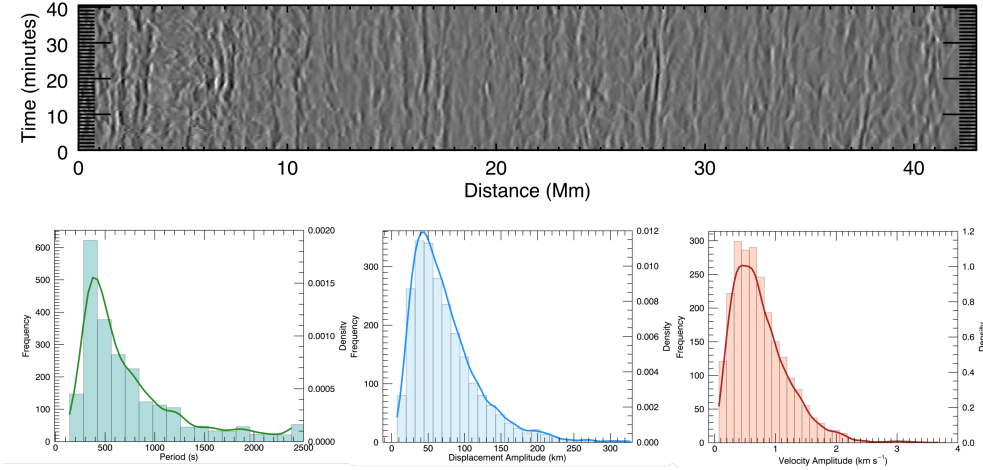


Figure 8. Example time-distance diagram of super-penumbral fibrils. The transverse displacement of the fibrils is evident, with a number showing near sinusoidal displacements. The figure is generated from an arc-shaped cross-cut, with a radius of 12 Mm and centred on the sunspot bary-centre. The data has been unsharp masked. The bottom row displays summary plots of the transverse wave properties: period (left), displacement amplitude (middle) and velocity amplitude (right). Each panel displays the histogram, binned using Scott’s rule, and the kernel density estimate (solid line) with the bandwidth selected using Silverman’s rule.

Figure 8 (bottom panels) display summary plots of the basic properties of the transverse motions from the NUWT results, namely displacement and velocity amplitude, and period. A statistical summary of the measures of centre and spread are also given in Table 1. The typical displacements found here are broadly in agreement with those found in other chromospheric fibrils ([Morton *et al.* 2013](#); [Jess *et al.* 2015](#); [Jafarzadeh *et al.* 2017](#)), however the central measures for the periods and velocity amplitudes are larger and smaller, respectively, compared to the previously reported values. The dominance of longer periods here could be attributed to the relatively long cadence of the current data set (in comparison to previous studies), meaning we cannot sample the parameter space effectively. Furthermore, given that velocity amplitude and period show a negative correlation⁷, the inability to properly measure the higher frequency waves would lead to a reduction in the central measures for velocity amplitude. This speculation would need to be confirmed with higher cadence data sets.

⁷ This trend has also been reported previously in studies of both chromospheric ([Morton *et al.* 2013](#)), and coronal ([Morton *et al.* 2019](#)) transverse waves.

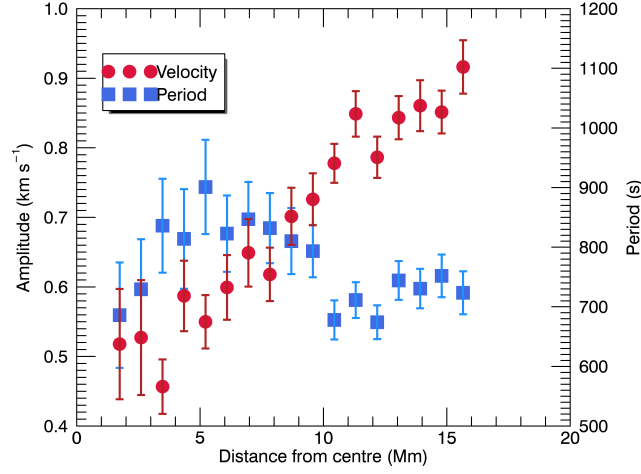


Figure 9. Wave properties as a function of distance from the umbral centre. The figure displays the mean values for velocity and period, with the error bars denoting the standard errors on the mean.

Finally, we show an interesting result that requires further investigation but will be left to a future study. Figure 9 displays the mean velocity amplitude of the transverse waves as a function of distance from the umbral bary-centre. The mean values are calculated from all measurements obtained in an individual arc. The measurements show that the mean value of the wave amplitude increases with distance from the sunspot centre. Assuming that the wave propagation can be suitably described by WKB theory, then the variation in amplitude, v , can be associated with a change in density, ρ . The velocity amplitude is expected to vary as, $v \propto \rho^{-1/4}$ (assuming the waves are Alfvénic, see Morton 2014). Hence, an increase in v suggests that the density decreases along the fibrils. This is perhaps not unexpected, as the super-penumbral fibrils are likely tracing the magnetic field as it rises out of the sunspot umbra and re-connecting with the solar surface at some distance from the spot (apparently outside of the current SST field of view). It is naturally expected that the density would decrease with height. Given the inverse relationship found between period and velocity amplitude, mentioned previously, we also show the mean period in Figure 9. The mean value of period is consistent with a constant value as a function of radius, within 2 standard errors. Hence, the observed change in wave amplitude is not due to a change in the populations of waves being measured.

5. DISCUSSION AND CONCLUSIONS

We have demonstrated a range of MHD wave phenomenon are present within the chromosphere of the sunspot under observation. However, our primary focus is on the transverse motions of the super-penumbral fibrils, which we have interpreted as signatures of transverse waves, namely the MHD kink mode. This is not the the first observation of transverse wave modes in the chromosphere (e.g., Jess *et al.* 2015), or even the first report of such waves in super-penumbral fibrils (Pietarila *et al.* 2011). Here we have demonstrated that, like seemingly everywhere else in the chromosphere, transverse waves modes pervade the sunspot chromosphere. We also characterised the properties of the super-penumbral transverse waves through a large-scale study. The presence of ubiquitous transverse waves in the sunspot atmosphere raises immediate questions about the nature of their excitation. The answer to these questions could provide important insights into the flow of energy through the lower atmosphere. We discuss the potential candidates in the following.

5.1. Convection-driven

Conventionally, transverse modes are expected to be driven by convective motions buffeting magnetic field concentrations in the photosphere, with evidence for this relationship between photospheric granular motions and chromospheric waves in the quiet Sun (Morton *et al.* 2013). However, the strong magnetic field that forms within the sunspot acts to suppress the convective motions, with the suppression especially evident in the umbra. The strong field is also thought to modify convection at the periphery of the spot, forming the penumbra and leading to a highly directional convection. Moreover, the measured properties of the transverse waves here reveal typically larger periods and smaller velocity amplitudes than their quiet Sun counterparts. If one were to assume that convection drove the transverse waves with the same energy as in the quiet Sun, the differences in velocity amplitude could be attributed to stronger magnetic fields in the sunspot. On the other hand, the difference in typical periods could indicate a non-convective excitation. As mentioned, we note that we do not believe that we are able to effectively measure high frequency waves; hence the measured distribution (Figure 8) might not reflect the true distribution of periods. Given the modified convection within the sunspot, this raises the question as to whether another mechanism might be dominant in exciting the transverse modes found along the super-penumbral fibrils?

5.2. Mode-conversion

As discussed in the introduction, mode conversion is expected to be a natural feature in the sunspot. It is now well established (at least numerically) that p -modes can convert to either slow or fast magnetoacoustic waves at the equipartition layer, depending upon the local inclination of the magnetic field (e.g., Bogdan *et al.* 2003; Khomenko and Collados 2006; Schunker and Cally 2006). The model of Khomenko and Cally (2012) suggests that the generation of upward propagating fast modes is most efficient for inclinations of 30° - 60° (c.f. their Figure 5). Such values are consistent with the inclination of the super-penumbral magnetic field estimated through the slow wave magneto-seismology (Figure 3). Additionally, it is expected that in sunspot atmospheres, the fast modes generated at the equipartition layer are reflected due to gradients in the Alfvén speed near the transition region. Although it is worth noting that, to date, the models that examine wave propagation in sunspots do not incorporate the inhomogeneous plasma structures observed in the chromosphere, i.e., the super-penumbral fibrils. The lack of small-scale waveguides in the simulations means that the fast mode propagation is not restricted to follow magnetic field lines. This is not the case for structured media, where fast mode wave energy can be ‘trapped’ within density enhancements and hence will follow the magnetic field (e.g., Van Doorsselaere *et al.* 2008). This could imply that a fraction of the fast mode wave energy are not reflected along the inclined field lines, as they do not reach the transition region; instead are siphoned along the chromospheric fine structure.

Furthermore, a number of recent theoretical and numerical investigations have shown that, the p -mode-excited fast magnetoacoustic modes can convert to Alfvénic modes at regions where sharp gradients in Alfvén speed exist, e.g., near the transition region (Cally 2011; Khomenko and Cally 2012). There are indications that this latter mode conversion is responsible for part of the coronal flux of Alfvénic waves (Cally 2017; Morton *et al.* 2019). Whether this would be relevant for wave excitation along the superpenumbral fibrils is still unclear.

The transverse motions that we observe can be described by the kink mode. The kink mode can have qualities that means it is often described as Alfvénic in character (e.g., Goossens *et al.* 2012),

although it is still considered to be a fast magnetoacoustic mode (e.g., De Moortel and Nakariakov 2012). Given the hybrid nature of the mode, it is possible that it could be excited at either the equipartition layer or at the transition region. However, only the former situation would seemingly agree with our observation. The analysis suggests that the waves are propagating in the chromosphere and away from the umbra, hence seemingly excited from below.

It is also worth providing a crude estimate of the wave energy in order to evaluate whether mode-conversion from p -modes is a valid candidate. The time average energy in the transverse modes can be approximated as:

$$E = \frac{1}{2} \rho v^2 v_A. \quad (4)$$

We use the Alfvén speed, v_A , as opposed to the kink speed, in order to provide straightforward estimates for the wave propagation speed from values of B and ρ obtained through various methods. Given the uncertainties with the following estimate, the difference between using the kink speed and v_A is negligible. The magnetic field strength in the super-penumbral fibrils is on the order of 300-400 G (Asensio Ramos *et al.* 2017) and density estimates for chromospheric plasma at a height of ~ 1300 km is $\sim 1.3 \times 10^{-8} \text{ kg m}^{-3}$ (Maltby *et al.* 1986). Using these values gives an Alfvén speed between 200-300 km s^{-1} . We note this is around 10 times the propagation speed we are able to measure (Table 1). The reason for this significant difference is a mystery to us. As mentioned, Jafarzadeh *et al.* (2017) also report small propagation speeds in fibrils in an active region.

Given the disparity in expected and measured speeds, we have a broad range for v_A possible (20-300 km s^{-1}). Energy fluxes are calculated to be somewhere between $E = 80 - 1200 \text{ W m}^{-2}$, using the mean value of velocity amplitude (Table 1). These values are broadly consistent with the amount of energy found in fast-modes through mode conversion from the simulations of Khomenko and Cally (2012), $\sim 300 \text{ W m}^{-2}$.

5.3. Reconnection driven

A final alternative is wave excitation via magnetic reconnection. Pietarila *et al.* (2011) analyse a single transverse wave event that demonstrates a relatively large amplitude (displacement ~ 150 km). Based upon other indicators in their data set, the authors suggest that the wave was driven by a reconnection event. Moreover, various studies have demonstrated that there are potentially a significant number of reconnection events in the penumbra that lead to the presence of ‘jets’ in the penumbral chromosphere (Katsukawa *et al.* 2007). These so called penumbral microjets are typically short in length and the associated enhancement of emission in Ca II lines is short-lived (1–2 minutes - Vissers *et al.* 2015; Drews and Rouppe van der Voort 2017). However, evidence seems to suggest there is little mass-motion associated with these features and they are potentially heating fronts associated with reconnection occurring lower in the atmosphere (Esteban Pozuelo *et al.* 2019; Rouppe van der Voort and Drews 2019; Drews and Rouppe van der Voort 2020). At present, it is unclear whether there is a connection between the occurrence of these microjets and the transverse waves - although the current data set may enable such a comparison to take place.

5.4. Conclusions

The results presented here confirm the ubiquity of transverse wave motions throughout the chromosphere, adding sunspot super-penumbral fibrils to the increasing list of structures found to host the waves. However, their very presence in the super-penumbral fibrils raises questions about their

excitation that might not be asked about the transverse waves found in other chromospheric features. Considering the options, we suggest mode conversion is the underlying mechanism that leads to the transverse waves in sunspots. We expect further investigation with higher cadence data will help shed some light on this.

ACKNOWLEDGMENTS

R.J.M acknowledges UKRI for support under the Future Leaders Fellowship MR/T019891/1. V.M.J.H would like to acknowledge support through the Research Council of Norway, project number 250810, and through its Centers of Excellence scheme, project number 262622. He also benefited from funding from the European Research Council (ERC) under the European Union’s Horizon 2020 research and innovation programme (grant agreement No. 682462). We are deeply indebted to H. Socas-Navarro for continuously making his inversion code available to the community.

REFERENCES

- B. De Pontieu, R. Erdélyi, and S. P. James, *Nature* **430**, 536 (2004)
- B. De Pontieu, S. W. McIntosh, M. Carlsson, V. H. Hansteen, T. D. Tarbell, C. J. Schrijver, A. M. Title, R. A. Shine, S. Tsuneta, Y. Katsukawa, K. Ichimoto, Y. Suematsu, T. Shimizu, and S. Nagata, *Science* **318**, 1574 (2007)
- S. Tomczyk, S. W. McIntosh, S. L. Keil, P. G. Judge, T. Schad, D. H. Seeley, and J. Edmondson, *Science* **317**, 1192 (2007)
- D. B. Jess, M. Mathioudakis, R. Erdélyi, P. J. Crockett, F. P. Keenan, and D. J. Christian, *Science* **323**, 1582 (2009), [arXiv:0903.3546](#)
- S. W. McIntosh, B. de Pontieu, M. Carlsson, V. Hansteen, P. Boerner, and M. Goossens, *Nature* **475**, 477 (2011)
- R. J. Morton, G. Verth, J. A. McLaughlin, and R. Erdélyi, *ApJ* **744**, 5 (2012a), [arXiv:1109.4851 \[astro-ph.SR\]](#)
- R. J. Morton, S. Tomczyk, and R. Pinto, *Nature Communications* **6**, 7813 (2015)
- R. J. Morton, M. J. Weberg, and J. A. McLaughlin, *Nature Astronomy* **3**, 223 (2019), [arXiv:1902.03811 \[astro-ph.SR\]](#)
- B. E. Goldstein, E. J. Smith, A. Balogh, T. S. Horbury, M. L. Goldstein, and D. A. Roberts, *Geophysical Research Letters* **22**, 3393 (1995)
- M. Goossens, J. Andries, R. Soler, T. Van Doorsselaere, I. Arregui, and J. Terradas, *ApJ* **753**, 111 (2012), [arXiv:1205.0935 \[astro-ph.SR\]](#)
- T. J. Okamoto and B. De Pontieu, *ApJL* **736**, L24 (2011), [arXiv:1106.4270 \[astro-ph.SR\]](#)
- R. J. Morton, G. Verth, D. B. Jess, D. Kuridze, M. S. Ruderman, M. Mathioudakis, and R. Erdélyi, *Nature Communications* **3**, 1315 (2012b), [arXiv:1306.4124 \[astro-ph.SR\]](#)
- M. J. Weberg, R. J. Morton, and J. A. McLaughlin, *The Astrophysical Journal* **894**, 79 (2020)
- S. R. Cranmer and A. A. van Ballegooijen, *ApJS* **156**, 265 (2005), [arXiv:astro-ph/0410639](#)
- P. S. Cally, *MNRAS* **466**, 413 (2017), [arXiv:1612.02064 \[astro-ph.SR\]](#)
- S. R. Cranmer, *The Astrophysical Journal* **862**, 6 (2018)

- P. S. Cally, in *Astronomical Society of India Conference Series*, Astronomical Society of India Conference Series, Vol. 2 (2011) pp. 221–227
- P. S. Cally and S. C. Hansen, *ApJ* **738**, 119 (2011)
- E. Khomenko and P. S. Cally, *ApJ* **746**, 68 (2012)
- T. J. Bogdan and P. G. Judge, *Philosophical Transactions of the Royal Society of London Series A* **364**, 313 (2006)
- D. B. Jess, R. J. Morton, G. Verth, V. Fedun, S. D. T. Grant, and I. Giagkiozis, *SSRv* **190**, 103 (2015)
- D. B. Jess, B. Snow, S. J. Houston, G. J. J. Botha, B. Fleck, S. Krishna Prasad, A. Asensio Ramos, R. J. Morton, P. H. Keys, S. Jafarzadeh, M. Stangalini, S. D. T. Grant, and D. J. Christian, *Nature Astronomy* **4**, 220 (2019)
- J. H. Thomas, L. E. Cram, and A. H. Nye, *The Astrophysical Journal* **285**, 368 (1984)
- B. W. Lites and J. H. Thomas, *The Astrophysical Journal* **294**, 682 (1985)
- N. Brynildsen, O. Kjeldseth-Moe, P. Maltby, and K. Wilhelm, *The Astrophysical Journal* **517**, L159 (1999)
- L. H. M. Rouppe van der Voort, R. J. Rutten, P. Sütterlin, P. J. Sloover, and J. M. Krijger, *A&A* **403**, 277 (2003)
- H. Tian, E. DeLuca, K. K. Reeves, S. McKillop, B. De Pontieu, J. Martínez-Sykora, M. Carlsson, V. Hansteen, L. Kleint, M. Cheung, L. Golub, S. Saar, P. Testa, M. Weber, J. Lemen, A. Title, P. Boerner, N. Hurlburt, T. D. Tarbell, J. P. Wuelser, C. Kankelborg, S. Jaeggli, and S. W. McIntosh, *ApJ* **786**, 137 (2014), [arXiv:1404.6291 \[astro-ph.SR\]](#)
- R. G. Giovanelli, *Solar Physics* **27**, 71 (1972)
- D. S. Bloomfield, A. Lagg, and S. K. Solanki, *ApJ* **671**, 1005 (2007), [arXiv:0709.3731](#)
- W. F. Briskin and H. Zirin, *ApJ* **478**, 814 (1997)
- N. I. Kobanov and D. V. Makarchik, *A&A* **424**, 671 (2004)
- D. B. Jess, V. E. Reznikova, T. Van Doorselaere, P. H. Keys, and D. H. Mackay, *The Astrophysical Journal* **779**, 168 (2013)
- N. Bel and B. Leroy, *A&A* **55**, 239 (1977)
- H. Schunker and P. S. Cally, *MNRAS* **372**, 551 (2006)
- E. Khomenko and M. Collados, *ApJ* **653**, 739 (2006)
- T. M. Brown, T. J. Bogdan, B. W. Lites, and J. H. Thomas, *ApJL* **394**, L65 (1992)
- E. Khomenko and M. Collados, *Astronomy & Astrophysics* **506**, L5 (2009)
- G. B. Scharmer, K. Bjelksjo, T. K. Korhonen, B. Lindberg, and B. Petterson, in *Innovative Telescopes and Instrumentation for Solar Astrophysics*, Proc. SPIE, Vol. 4853, edited by S. L. Keil and S. V. Avakyan (2003) pp. 341–350
- G. B. Scharmer, *A&A* **447**, 1111 (2006)
- G. B. Scharmer, G. Narayan, T. Hillberg, J. de la Cruz Rodriguez, M. G. Löfdahl, D. Kiselman, P. Sütterlin, M. van Noort, and A. Lagg, *ApJL* **689**, L69 (2008), [arXiv:0806.1638](#)
- V. M. J. Henriques, M. Mathioudakis, H. Socas-Navarro, and J. d. I. C. Rodríguez, *The Astrophysical Journal* **845**, 102 (2017)
- J. de la Cruz Rodríguez, M. G. Löfdahl, P. Sütterlin, T. Hillberg, and L. Rouppe van der Voort, *A&A* **573**, A40 (2015)
- M. van Noort, L. Rouppe van der Voort, and M. G. Löfdahl, *SoPh* **228**, 191 (2005)

- V. M. J. Henriques, *A&A* **548**, A114 (2012)
- R. A. Shine, A. M. Title, T. D. Tarbell, K. Smith, Z. A. Frank, and G. Scharmer, *ApJ* **430**, 413 (1994)
- C. B. Markwardt, in *Astronomical Data Analysis Software and Systems XVIII*, ASPCS, Vol. 411, edited by D. A. Bohlender, D. Durand, and P. Dowler (2009) p. 251, [arXiv:0902.2850 \[astro-ph.IM\]](#)
- G. Cauzzi, K. Reardon, R. J. Rutten, A. Tritschler, and H. Uitenbroek, *A&A* **503**, 577 (2009), [arXiv:0906.2083 \[astro-ph.SR\]](#)
- J. Löhner-Böttcher, *Wave phenomena in sunspots*, Ph.D. thesis, Universität Freiburg im Breisgau (2016)
- H. Socas-Navarro, J. de la Cruz Rodríguez, A. Asensio Ramos, J. Trujillo Bueno, and B. Ruiz Cobo, *A&A* **577**, A7 (2015), [arXiv:1408.6101 \[astro-ph.SR\]](#)
- J. M. Fontenla, E. H. Avrett, and R. Loeser, *The Astrophysical Journal* **406**, 319 (1993)
- V. M. J. Henriques, C. J. Nelson, L. H. M. Rouppe van der Voort, and M. Mathioudakis, *arXiv e-prints*, [arXiv:2008.05482 \(2020\)](#), [arXiv:2008.05482 \[astro-ph.SR\]](#)
- J. de la Cruz Rodríguez and N. Piskunov, *The Astrophysical Journal* **764**, 33 (2013)
- J. Leenaarts, J. de la Cruz Rodríguez, O. Kochukhov, and M. Carlsson, *The Astrophysical Journal* **784**, L17 (2014)
- S. Bose, V. M. J. Henriques, L. R. van der Voort, and T. M. D. Pereira, *Astronomy & Astrophysics* **627**, A46 (2019)
- A. Asensio Ramos, J. de la Cruz Rodríguez, M. J. Martínez González, and H. Socas-Navarro, *A&A* **599**, A133 (2017), [arXiv:1612.06088 \[astro-ph.SR\]](#)
- T. A. Schad, M. J. Penn, and H. Lin, *The Astrophysical Journal* **768**, 111 (2013)
- T. A. Schad, M. J. Penn, H. Lin, and A. Tritschler, *Solar Physics* **290**, 1607 (2015)
- R. J. Morton, *A&A* **566**, A90 (2014)
- R. J. Morton, G. Verth, A. Hillier, and R. Erdélyi, *ApJ* **784**, 29 (2014), [arXiv:1310.4650 \[astro-ph.SR\]](#)
- K. Moorooogen, R. J. Morton, and V. Henriques, *A&A* **607**, A46 (2017), [arXiv:1708.03500 \[astro-ph.SR\]](#)
- S. Jafarzadeh, S. K. Solanki, R. Gafeira, M. van Noort, P. Barthol, J. Blanco Rodríguez, J. C. del Toro Iniesta, A. Gandorfer, L. Gizon, J. Hirzberger, M. Knölker, D. Orozco Suárez, T. L. Riethmüller, and W. Schmidt, *ApJS* **229**, 9 (2017), [arXiv:1610.07449 \[astro-ph.SR\]](#)
- D. Kuridze, G. Verth, M. Mathioudakis, R. Erdélyi, D. B. Jess, R. J. Morton, D. J. Christian, and F. P. Keenan, *ApJ* **779**, 82 (2013)
- A. Pietarila, R. Aznar Cuadrado, J. Hirzberger, and S. K. Solanki, *ApJ* **739**, 92 (2011)
- R. Gafeira, A. Lagg, S. K. Solanki, S. Jafarzadeh, M. van Noort, P. Barthol, J. Blanco Rodríguez, J. C. del Toro Iniesta, A. Gandorfer, L. Gizon, J. Hirzberger, M. Knölker, D. Orozco Suárez, T. L. Riethmüller, and W. Schmidt, *ApJS* **229**, 6 (2017), [arXiv:1612.00319 \[astro-ph.SR\]](#)
- J. Chae, H. Yang, H. Park, R. Ajor Maurya, K.-S. Cho, and V. Yurchyshyn, *ApJ* **789**, 108 (2014)
- J. Chae, D. Song, M. Seo, K.-S. Cho, Y.-D. Park, and V. Yurchyshyn, *ApJL* **805**, L21 (2015)
- J. Leenaarts, M. Carlsson, and L. Rouppe van der Voort, *ApJ* **802**, 136 (2015)
- M. J. Weberg, R. J. Morton, and J. A. McLaughlin, *ApJ* **852**, 57 (2018)

- R. J. Morton, G. Verth, V. Fedun, S. Shelyag, and R. Erdélyi, *ApJ* **768**, 17 (2013), [arXiv:1303.2356 \[astro-ph.SR\]](#)
- T. J. Bogdan, M. Carlsson, V. H. Hansteen, A. McMurry, C. S. Rosenthal, M. Johnson, S. Petty-Powell, E. J. Zita, R. F. Stein, S. W. McIntosh, and Å. Nordlund, *ApJ* **599**, 626 (2003)
- E. Khomenko and M. Collados, *The Astrophysical Journal* **653**, 739 (2006)
- E. Khomenko and P. S. Cally, *The Astrophysical Journal* **746**, 68 (2012)
- T. Van Doorselaere, C. S. Brady, E. Verwichte, and V. M. Nakariakov, *A&A* **491**, L9 (2008)
- I. De Moortel and V. M. Nakariakov, *Philosophical Transactions of the Royal Society of London Series A* **370**, 3193 (2012), [arXiv:1202.1944 \[astro-ph.SR\]](#)
- P. Maltby, E. H. Avrett, M. Carlsson, O. Kjeldseth-Moe, R. L. Kurucz, and R. Loeser, *ApJ* **306**, 284 (1986)
- Y. Katsukawa, T. E. Berger, K. Ichimoto, B. W. Lites, S. Nagata, T. Shimizu, R. A. Shine, Y. Suematsu, T. D. Tarbell, A. M. Title, and S. Tsuneta, *Science* **318**, 1594 (2007)
- G. J. M. Vissers, L. H. M. Rouppe van der Voort, and M. Carlsson, *The Astrophysical Journal* **811**, L33 (2015)
- A. Drews and L. Rouppe van der Voort, *Astronomy & Astrophysics* **602**, A80 (2017)
- S. Esteban Pozuelo, J. de la Cruz Rodríguez, A. Drews, L. Rouppe van der Voort, G. B. Scharmer, and M. Carlsson, *The Astrophysical Journal* **870**, 88 (2019)
- L. H. M. Rouppe van der Voort and A. Drews, *Astronomy & Astrophysics* **626**, A62 (2019)
- A. Drews and L. Rouppe van der Voort, *arXiv e-prints*, [arXiv:2005.02608](#) (2020), [arXiv:2005.02608 \[astro-ph.SR\]](#)